IDENTIFICATION OF DAMAGE MODEL WITH CRACKS FROM RESULTS OF THREE-POINT BENDING TEST

A. Kučerová[*] **, D. Brancherie**[†] **, A. Ibrahimbegović**[‡]

Summary: *Presented paper is concerned with the numerical modeling of quasi-brittle materials such as concrete. Brancherie and Ibrahimbegovic are authors of a simple model capable of describing the behavior of a structure until localized failure. In this paper, we discuss the identification of the model parameters from results of the three-point bending test. This leads to an optimization problem, which is solved by the stochastic algorithm based on an adaptive approximation of the objective function by the Radial Basis Function Network dynamically evolved by minima located by a real-encoded genetic algorithm.*

1 Introduction

Concrete is very frequently used material in the civil engineering. It could be considered as a quasi-brittle material with very complex mechanical behavior. Brancherie and Ibrahimbegovic are authors of a relatively simple model capable of describing the behavior of a massive structure until the point of localized failure. The model contains all the ingredients for taking into account both the diffuse damage mechanism, which leads to the appearance of microcracks, as well as the failure process characterized by the propagation of macrocracks. Perhaps the most important advantage of the proposed model is the fact that all its parameters have a clear physical interpretation and can be straightforwardly visualized in terms of the shape of a stress-strain diagram. In addition, influence of each parameter is dominant only for specific, easily recognizable, stages of material behavior. This kind of a priori knowledge has a potential to greatly simplify the model calibration and will be systematically used throughout the paper.

In this paper, we discuss the identification of the model parameters from experimental measurements made on a structural level. Generally speaking, the complexity of the identification procedure is determined by the choice of experimental setup. Solely from the identification point of view, the simplest experiment to execute is the uniaxial tensile test. In this case, the strain field stays mostly homogeneous during the whole procedure and the global response represented by the load-displacement diagram is very similar to the stress-strain curve

---

[*] Ing. Anna Kučerová: Department of Mechanics, Faculty of Civil Engineering, Czech Technical University in Prague, Thákurova 7, 166 29 Prague 6, tel: (+420)-2-2435-4369, fax: (+420)-2-2431-077, e-mail: anicka@cml.fsv.cvut.cz

[†] Delphine Brancherie: Université de Technologie de Compiègne, Compiègne, France

[‡] Adnan Ibrahimbegović: Laboratoire de mécanique et technologie, Ecole Normale Supérieure de Cachan, Cachan, France

for one material point. The model parameters can be then directly determined from the shape of the load-displacement curve. Such a uniform loading is, however, very difficult to impose in a laboratory test, especially for quasi-brittle materials. Therefore, other tests are often used in experimental practice.

The three-point bending test, in particular, is considered to be much simpler to perform and its results are well-reproducible. Therefore, we focus on the identification procedure for the proposed model parameters directly from results of the three-point bending test. Main difficulty is in this case imposed by heterogeneity of the stress and the strain fields, which is present since the very start of the experiment. The macro-scale measurements provide the load-deflection curve that integrates data from different parts of the specimen experiencing different regimes of (in)elastic behavior. For that reason, the possibility of a simple determination of model parameters from load-deflection curve is lost and an advanced calibration procedure needs to be applied.

To take advantage of the model specific structure, already mentioned above, the identification procedure should be divided into three sequential stages discussed in detail in Section 3. From the algorithmic point of view, the material calibration can then be understood as a sequential optimization problem. Such approach has two main advantages: first, solving three simpler identification steps in a batch form is typically much more efficient then the full-scale problem; second, it allows to use only a subset of simulations for initial stages of identification process.

The gradient-based methods are usually considered to be the most computationally efficient optimization algorithms available and as such have been successfully used in a variety of identification problems, e.g. (9). For the current model, however, analytic determination of sensitivities is fairly difficult, mainly due the history dependency of the model as well as complex interaction of individual parameters. The accuracy of numerical approximation to the "exact" sensitivities, on the other hand, is driven by the choice of pseudo-time step used in numerical simulations. Clearly, to reduce the computational time, the pseudo-time step should be used as large as possible. Therefore, the response-based objective function will not be smooth and gradient-based methods are unlikely to be very successful.

As an alternative, techniques of soft-computing can be employed for optimization of complex objective functions. For example, stochastic evolutionary algorithms have been successfully used for solution of identification problems on a level of material point (4) or on a level of simple structures (10; 16). For the current case, however, complexity of the optimization can be attributed rather to its non-smooth character than to the appearance of multiple optima; the family of problems where evolutionary algorithms are the most successful methods. This opens the way to more specialized tools, which deliver higher efficiency when compared to usually time-consuming evolutionary algorithms.

The approach adopted in the present work is based on an adaptive smoothing of the objective function by artificial neural networks (see, e.g., (20) for alternative ANN-based solutions to identification problems). In particular, the approximated model is provided by the Radial Basis Function Network, described in Section 4.2, dynamically evolved by minima located by a real-encoded genetic algorithm, briefly reviewed in Section 4.1. The proposed sequential numerical strategy is systematically verified in Section 5 with attention paid to a detailed assessment of the proposed stochastic algorithm reliability. Final remarks and conclusions can be found in Section 6.

2 A brief description of the identified model

In the present section, we give a brief description of the model on which the identification procedure is based. As already mentioned, the proposed model is capable of taking into account two different types of dissipation (e.g. see (11)):

- a bulk dissipation induced by the appearance of uniformly distributed microcracks. This bulk dissipation is taken into account by the use of a classical continuum damage model;

- a surface dissipation induced by the development of macrocracks responsible for the collapse of the structure. This phase is taken into account by the use of a strong discontinuity model. The surface dissipation is taken into account by the introduction of a traction/displacement jump relation.

Therefore, two different models are involved in the constitutive description: the one associated with the bulk material and the one associated with the displacement discontinuity. Both are built on the same scheme considering the thermodynamics of continuous media and interfaces.

The key points of the construction of each of the two models are summarized in Table 1 and Table 2.

Helmholtz energy	$\bar{\psi}(\bar{\varepsilon}, \overline{\mathbf{D}}, \bar{\xi}) = \frac{1}{2}\bar{\varepsilon} : \overline{\mathbf{D}}^{-1} : \bar{\varepsilon} + \bar{\Xi}(\bar{\xi})$
Damage function	$\bar{\phi}(\boldsymbol{\sigma}, \bar{q}) = \underbrace{\sqrt{\boldsymbol{\sigma} : \mathbf{D}^e : \boldsymbol{\sigma}}}_{\|\boldsymbol{\sigma}\|_{\mathbf{D}^e}} - \frac{1}{\sqrt{E}}(\sigma_f - \bar{q})$
State equations	$\boldsymbol{\sigma} = \overline{\mathbf{D}}^{-1} : \bar{\varepsilon} \quad \text{and} \quad \bar{q} = -\frac{d}{d\bar{\xi}}\bar{\Xi}(\bar{\xi})$
Evolution equations	$\dot{\overline{\mathbf{D}}} = \dot{\bar{\gamma}}\frac{\partial\bar{\phi}}{\partial\boldsymbol{\sigma}} \otimes \frac{\partial\bar{\phi}}{\partial\boldsymbol{\sigma}}\frac{1}{\|\boldsymbol{\sigma}\|_{\mathbf{D}^e}} \quad ; \quad \dot{\bar{\xi}} = \dot{\bar{\gamma}}\frac{\partial\bar{\phi}}{\partial\bar{q}}$
Dissipation	$0 \leqslant \bar{\mathcal{D}} = \frac{1}{2}\dot{\bar{\xi}}(\bar{\sigma}_f - \bar{K}\bar{\xi})$

Table 1: Main ingredients of the continuum damage model

Helmholtz energy	$\bar{\bar{\psi}}(\bar{\mathbf{u}}, \bar{\mathbf{Q}}, \bar{\bar{\xi}}) = \frac{1}{2}\bar{\bar{\mathbf{u}}} \cdot \bar{\mathbf{Q}}^{-1} \cdot \bar{\bar{\mathbf{u}}} + \bar{\bar{\Xi}}(\bar{\bar{\xi}})$
Damage functions	$\bar{\bar{\phi}}_1(\mathbf{t}_{\Gamma_s}, \bar{\bar{q}}) = \mathbf{t}_{\Gamma_s} \cdot \mathbf{n} - (\bar{\bar{\sigma}}_f - \bar{\bar{q}})$ $\bar{\bar{\phi}}_2(\mathbf{t}_{\Gamma_s}, \bar{\bar{q}}) = |\mathbf{t}_{\Gamma_s} \cdot \mathbf{m}| - (\bar{\bar{\sigma}}_s - \frac{\bar{\bar{\sigma}}_s}{\bar{\bar{\sigma}}_f}\bar{\bar{q}})$
State equations	$\mathbf{t}_{\Gamma_s} = \bar{\mathbf{Q}}^{-1} \cdot \bar{\bar{\mathbf{u}}} \quad \text{and} \quad \bar{\bar{q}} = -\frac{\partial\bar{\bar{\Xi}}}{\partial\bar{\bar{\xi}}}$
Evolution equations	$\dot{\bar{\mathbf{Q}}} = \dot{\bar{\bar{\gamma}}}_1\frac{1}{\mathbf{t}_{\Gamma_s} \cdot \mathbf{n}} + \dot{\bar{\bar{\gamma}}}_2\frac{1}{|\mathbf{t}_{\Gamma_s} \cdot \mathbf{m}|} \quad ; \quad \dot{\bar{\bar{\xi}}} = \dot{\bar{\bar{\gamma}}}_1 + \frac{\bar{\bar{\sigma}}_s}{\bar{\bar{\sigma}}_f}\dot{\bar{\bar{\gamma}}}_2$
Dissipation	$0 \leqslant \bar{\bar{\mathcal{D}}} = \frac{1}{2}\dot{\bar{\bar{\xi}}}(\bar{\bar{\sigma}}_f - \bar{K}\bar{\bar{\xi}})$

Table 2: Main ingredients of the discrete damage model

For the discrete damage model, the isotropic softening law is chosen as:

$$\bar{\bar{q}} = \bar{\bar{\sigma}}_f \left[1 - exp\left(-\frac{\bar{\bar{\beta}}}{\bar{\bar{\sigma}}_f}\bar{\bar{\xi}} \right) \right] \tag{1}$$

In Tables 1 and 2 the variables $\dot{\bar{\gamma}}$, $\dot{\bar{\bar{\gamma}}}_1$ and $\dot{\bar{\bar{\gamma}}}_2$ denote Lagrange multipliers induced by the use of the maximum dissipation principle. Moreover, $\bar{\bar{\mathbf{u}}}$ denotes the displacement jump on the surface of discontinuity. Finally, $\overline{\mathbf{D}}$ and $\bar{\bar{\mathbf{Q}}}$ correspond to the damaged compliance of the continuum and discrete model, respectively.

Note that in a three-point bending, the simulated response is almost independent of the limit tangential traction $\bar{\bar{\sigma}}_s$. Therefore, its value was set to $0.1\bar{\bar{\sigma}}_f$. With such simplification, there are six independent material parameters to be identified:

- the elastic parameters: the Young modulus E and the Poisson ratio ν;

- the continuum damage parameters: the limit stress $\bar{\sigma}_f$ and the hardening parameter $\bar{K}$;

- the discrete damage parameters: the limit normal traction $\bar{\bar{\sigma}}_f$ and the softening parameter $\bar{\bar{\beta}}$.

The limits of realistic values for each parameter are shown in Table 3. Note that in our identification methodology we do not suppose to have an expert capable of giving the initial estimate of material parameters values, as in e.g. (9; 19). Therefore, the bounds on model parameters were kept rather wide.

$$
\begin{array}{llllll}
E & \in & (25, 50)\,\text{GPa} & \bar{\sigma}_f & \in & (1, 5)\,\text{MPa} & \bar{\bar{\sigma}}_f & \in & (\bar{\sigma}_f{+}0.1, 2\bar{\sigma}_f)\,\text{MPa} \\
\nu & \in & (0.1, 0.4) & \bar{K} & \in & (10, 10000)\,\text{MPa} & \bar{\bar{\beta}} & \in & (0.1\bar{\bar{\sigma}}_f, 10\bar{\bar{\sigma}}_f)\,\text{MPa/mm}
\end{array}
$$

Table 3: Limits for the model parameters.

3 Optimization problem formulation

In the case of a three-point bending test the global response of a specimen represented by the load-deflection (L-u) diagram for the structure cannot be simply related to three-stage material response with elastic, hardening and softening part (see Figure 1a). Nevertheless, we assume that it will be still possible to employ the three-stage approach developed for the uniaxial tensile experiment in (14). The solution process will be divided into the optimization of elastic, hardening and softening parameters in the sequential way. Each step is described in detail in the rest of this section.

Due to lack of experimental data, a reference simulation with parameters shown in Table 4 will be used to provide the target data.

$$
\begin{array}{lllllll}
E & = & 38.0\,\text{GPa} & \bar{K} & = & 1000.0\,\text{MPa} & \bar{\bar{\sigma}}_f & = & 2.35\,\text{MPa} \\
\nu & = & 0.1 & \bar{\sigma}_f & = & 2.2\,\text{MPa} & \bar{\bar{\beta}} & = & 23.5\,\text{MPa/mm}
\end{array}
$$

Table 4: Parameter's values for reference simulation.

3.1 Identification of elastic parameters

In the elastic range, Young's modulus and Poisson's ratio are determined using very short simulations describing only the elastic response of a specimen represented by the linear part of load-deflection diagram. To identify both elastic parameters this information needs to be supplemented with an additional measurement. In particular, we propose to include the specimen
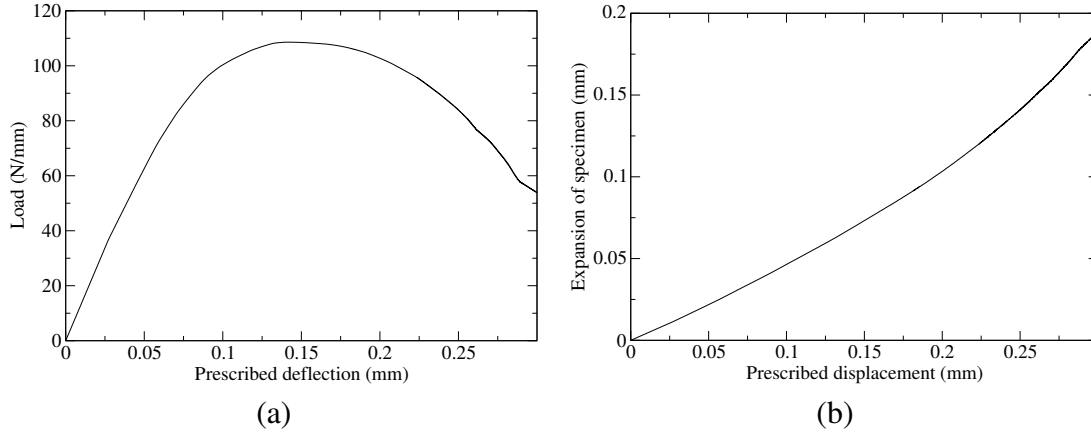
Figure 1: Three-point bending test: (a) Load-deflection diagram (b) Evolution of expansion of specimen.

expansion Δl defined as the relative horizontal displacements between the left and the right edge of the specimen (as indicated by arrows in Figure 2). The reference expansion-deflection curve is shown in Figure 1b.
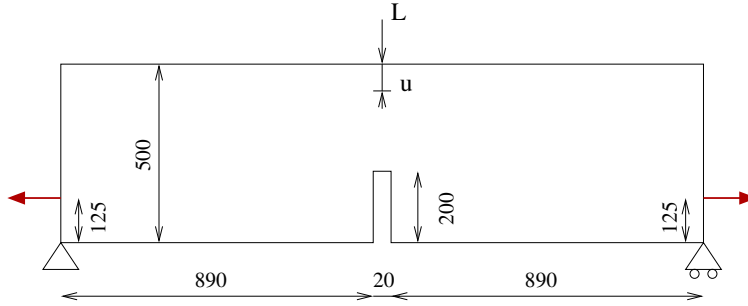

Figure 2: Displacements measured to evaluate the expansion Δl of the specimen.

The objective function F_1 applicable for the determination of elastic parameters can be defined as follows:

$$F_1 = (L_{ref}(u) - L(u))^2 w_1 + (\Delta l_{ref}(u) - \Delta l(u))^2 w_2 \quad ; \qquad u = 0.01\text{mm} \qquad (2)$$

The quantities with index $_{ref}$ correspond to the values taken from the reference diagram. The corresponding value of weights w_1 and w_2 were calculated using 30 random simulations to normalize the average value of each of summation terms in (2) to one.

3.2 Identification of hardening parameters

Once we have successfully determined Young's modulus and Poisson's ratio, we can continue towards the estimate of the elastic limit stress $\bar{\sigma}_f$ (representing a threshold of elastic behavior) and the hardening parameter $\bar{K}$. The limit stress will be related to the limit displacement $\bar{u}_f$ at the end of the linear part of the load-deflection diagram. The hardening parameter $\bar{K}$ will then govern the slope of the diagram in the hardening regime. In our particular case, the slope $\bar{s}$ is approximated as a secant determined from two distinct points. There are two contradictory requirements for that choice: first, the points should not be too close to $\bar{u}_f$ to ensure that numerical errors due to pseudo-time discretization do not exceed the impact of $\bar{K}$ parameter; second,

they should be close enough to $\bar{u}_f$ to ensure that the specimen does not enter the softening regime. The particular choice adopted in this work is

$$\bar{s} = (L(\bar{u}_f + 0.01\text{mm}) - L(\bar{u}_f + 0.005\text{mm}))/0.005\text{mm} \tag{3}$$

leading to the objective function in form

$$F_2 = (\bar{u}_{f,ref} - \bar{u}_f)^2 \, w_3 + (\bar{s}_{ref} - \bar{s})^2 \, w_4. \tag{4}$$

To keep this optimization step efficient, the simulations should again be restricted to a limited loading range, where the limit displacement can be related to the value of $\bar{u}_{f,ref}$ from the reference diagram. Note that during optimization process, there is no guarantee that $\bar{\sigma}_f$ will be exceeded when subjecting the specimen to the limit displacement. Such a solution is penalized by setting the objective function value to $10 \times N$, where $N = 2$ is the problem dimension, see Figure 3a. Moreover, as documented by Figure 3b, the objective function is now substantially noisy and hence more difficult to optimize.
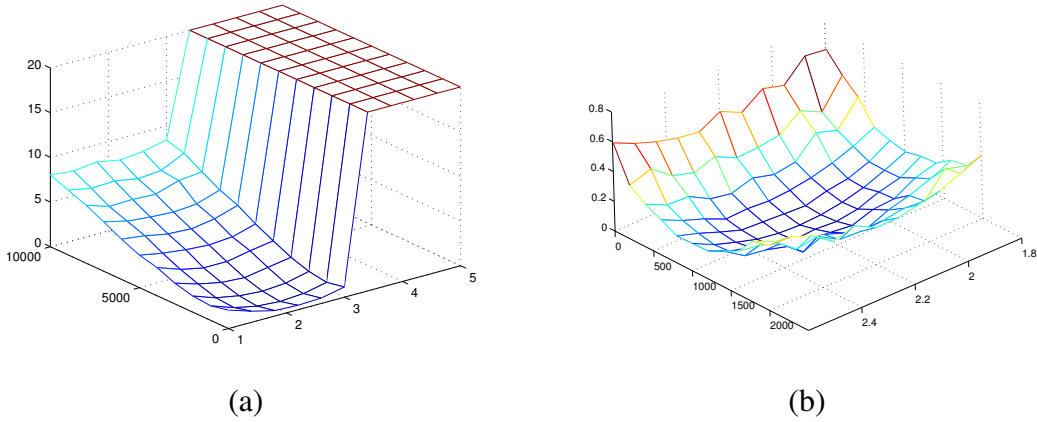

(a) (b)

Figure 3: Objective function F_2: (a) Whole domain (b) Detail close to optimum.

3.3 Identification of softening parameters

The last stage of identification involves the discrete damage parameters: the limit normal traction $\bar{\bar{\sigma}}_f$ and the softening parameter $\bar{\bar{\beta}}$. Variable $\bar{\bar{\sigma}}_f$ represents a limit of hardening of material and the appearance of a macroscopic crack. Determination of displacement $\bar{\bar{u}}_f$ corresponding to this event, however, is rather delicate. The most straightforward method is based on the comparison of the reference curve with a simulation for a very high value of $\bar{\bar{\sigma}}_f$. The point where these two curves start to deviate then defines the wanted value of $\bar{\bar{u}}_f$. A more reliable possibility could be based on a local optical measurement in the vicinity of notch (3) or acoustic emission techniques (2).

After the specimen enters the softening regime, the shape of diagram is fully governed by the softening parameter $\bar{\bar{\beta}}$. Therefore, its value can be fitted on the basis of the load corresponding to the deflection for which the softening is sufficiently active. This leads to the last objective function in the form

$$F_3 = (u_{f,ref}^{=} - \bar{\bar{u}}_f)^2 \, w_5 + (L_{ref}(u) - L(u))^2 \, w_6 \quad ; \qquad u = 0.15mm. \tag{5}$$

By analogy to the procedure described in the previous section, the penalization is applied to the cases where the specimen does not reach the softening regime until the end of simulations.

4 Optimization method

The algorithm used for the optimization of objective functions F_1, F_2 and F_3 is based on an efficient combination of an artificial neural network, namely the radial basis function network (RBFN), and an evolutionary algorithm **GRADE** extended by the niching strategy CERAF. The principle of the algorithm is the replacement of an objective function by a neural network approximation and its subsequent optimization by an evolutionary algorithm. The approximation is constructed on a basis of interpolation of several points, where the values of objective function were calculated exactly. The approximation is adaptively improved by new neurons (points), provided e.g. by optima located on the previous approximation.

The main advantage of this methodology is an inexpensive evaluation of the approximation, which is repeatedly used during stochastic optimization process. Computationally expensive objective function is evaluated only when new neurons are added to the neural network.

4.1 Evolutionary algorithm GRADE extended by strategy CERAF

Evolutionary algorithms nowadays belong to the most popular optimization tools. Unlike the traditional gradient optimization methods, evolutionary algorithms operate on a population (a set of possible solutions), applying 'genetic' operators (cross-over, mutation and selection). The principles of evolutionary algorithm were first proposed by Holland (8). Ever since, the evolutionary algorithms have reached wide application domain, see e.g. books by Goldberg (5) and Michalewicz (17) for an extensive review. In this work, we employ a **GRADE** algorithm (GRadient-based Atavistic Differential Evolution) developed in (10). The algorithmic scheme of the method is briefly summarized below.

The first step is to generate a starting generation of chromosomes by choosing random values of all state variables. The size of the population is in our case set to ten times the number of optimized variables. After the initiation stage the following steps are repeated until a termination condition is reached:

1. MUTATION, which creates a new solution $\boldsymbol{x}$ using the operation

$$\boldsymbol{x} = \boldsymbol{y} + k(\boldsymbol{y} - \boldsymbol{z}) , \qquad (6)$$

   where $\boldsymbol{y}$ is a solution from actual population, $\boldsymbol{z}$ is a randomly created solution and k is a real number from given bounds. Ten percents of solutions in a new population are created by this operator.

2. CROSS-OVER, which creates a new solution $\boldsymbol{x}$ according to

$$\boldsymbol{x} = \mathrm{opt}(\boldsymbol{y}, \boldsymbol{z}) + cs(\boldsymbol{y} - \boldsymbol{z}) , \qquad (7)$$

   where $\mathrm{opt}(\boldsymbol{y}, \boldsymbol{z})$ denotes a better solution from two randomly chosen vectors $\boldsymbol{y}$ and $\boldsymbol{z}$, c is a real random number with a uniform distribution on the interval [0;2] and s changes the direction of the descent $(\boldsymbol{y} - \boldsymbol{z})$ favor better solution from vectors $\boldsymbol{y}$ and $\boldsymbol{z}$. This operator creates 90% of individuals in a new population.

3. EVALUATION computes the objective function value for each new solution.

4. TOURNAMENT SELECTION, where the worst individual from two randomly selected solutions is deleted. This operator is repeated until the number of solution is the same as at the beginning of the cycle.

The basic version of **GRADE** is complemented with **CERAF** strategy (7) in order to increase the algorithm robustness when dealing with multi-modal problems. The **CERAF** strategy works on the principle of multi-start strategy supported with memory. If the best value found by a stochastic algorithm does not change for more than a prescribed value during a certain number of generations, **CERAF** store the optimal point in memory and surrounds it by a "radioactive" zone defined as n-dimensional ellipsoid with each diameter equal to 50% of the size of searched domain. If a new solution is located inside the 'radioactive" zone, it is replaced with a random one outside the zone. If this solution was created by the CROSS-OVER operator, the size of the 'radioactive" zone is decreased by 0.5% of the actual size. During the computations presented herein, the new local extreme was marked when the best value found had not changed for more than the stopping precision (defined as a property of objective function) during 100 generations. An interested reader is referred to (7) for more detailed description of **CERAF**.

4.2 Radial Basis Function Network

Artificial neural networks (ANNs) were initially developed to simulate the processes in a human brain and later generalized for many problems like pattern recognition, different approximations and predictions, control of systems, etc (21; 20). In this work, they will be used "only" as general approximation tools. The particular implementation is based on the idea of radial basis function networks as proposed e.g. in (18; 12).

Neural network replace the objective function $F(\mathbf{x})$ by approximation $\tilde{F}(\mathbf{x})$ defined as a sum of radial basis functions multiplied by synaptic weights:

$$F(\boldsymbol{x}) \approx \tilde{F}(\boldsymbol{x}) = \sum_{i=1}^{N} b_i(\boldsymbol{x}) w_i \,, \tag{8}$$

where $\boldsymbol{x}$ is a vector of unknowns, $b_i(\boldsymbol{x})$ is a basis function associated with i-th neuron, w_i is a weight of the i-th neuron and N is the total number of neurons creating the network. The basis function b_i has the following form

$$b_i(\boldsymbol{x}) = e^{-\|\boldsymbol{x}-\boldsymbol{c}_i\|^2/r} \,, \tag{9}$$

where $\boldsymbol{c}_i$ is a vector of the center coordinates for the i-th basis function and r is a normalizing factor set to

$$r = \frac{d_{max}}{\sqrt[D]{DN}} \,, \tag{10}$$

where d_{max} is the maximal distance within the domain and D is the number of dimensions.

Synaptic weights are computed from the condition

$$F(\boldsymbol{c}_i) = \tilde{F}(\boldsymbol{c}_i), \tag{11}$$

imposing the equality of the approximation and objective function values $\overline{y_i}$ in all neurons. This leads to a minimization problem in the form:

$$\min \sum_{i=1}^{N} [(\overline{y_i} - \sum_{j=1}^{N} b_j(\boldsymbol{c}_i) w_j)^2 + \lambda_i w_i^2] \,. \tag{12}$$

where λ_i is a regularization factor set to 10^{-7}. The solution of (12) leads to a system of linear equations determining the values of synaptic weights $\boldsymbol{w}$.

At this point, the RBFN approximation of the objective function is created and the above-mentioned evolutionary algorithm GRADE is used to locate the 'approximate' global optima. In the next step, to improve the quality of approximation, three new points are added into the neural network: the optimum of previous approximation, a random point and another point in the descent direction defined by optima found in two previous steps. A more detailed description of the method is available in (13).

In the current contest, one additional modification is introduced to deal with the penalization introduced in Sections 3.2 and 3.3. If the point to be added to the neural network is penalized, it is accepted only in the case, when it was the optimum found by evolutionary algorithm. The rationale behind this modification is to avoid the penalty-imposed discontinuities in the objective function, which are impossible to capture by the smooth RBFN approximation.

5   Identification procedure verification

When assessing the reliability of the proposed identification procedure a special care must be given to stochastic nature of the optimization algorithm. The analysis presented herein is based on the statistics of 100 independent optimization processes, executed for each objective function. The termination criteria were set to: first, the number of objective function evaluations exceeded 155; second, the value of objective function smaller than a stopping precision was found. A particular optimization process was marked as 'successful', when the latter termination condition was met. Note that since the reference simulation instead of experimental data is used, the optimum for every objective function is equal to zero. Results of the performance study are summarized in Table 5 showing the success rate related to a stopping precision together with the maximum and average number of function evaluations.

F	Stopping precision	Successful runs	Maximal number of F's evaluation	Average number of F's evaluation
F_1	10^{-3}	100	32	16
F_2	10^{-2}	94	140	29
F_2	10^{-3}	80	140	47
F_3	10^{-3}	92	140	37
F_3	3.10^{-3}	76	143	47

Table 5: Summary of reliability study.

Moreover, the different values of stopping precision allow us to investigate the relation between the accuracy of identified parameters and the tolerance of the objective function value. Table 6 shows a concrete outcome of such an analysis, where the maximal and average errors are calculated relatively to the size of the interval given by limit values for each parameter.

The results show that the maximal error for the elastic parameters E and ν is less than 3%, which is sufficient from the practical point of view. This is also documented by Figure 4, where no deviation of the reference and resulting curves is visible in the elastic range. For the hardening stage (parameters $\bar{\sigma}_f$ and $\bar{K}$) a similar precision is unfortunately not sufficient as shown by Figure 4a. Increasing the stopping precision to 10^{-3} reduces the error on parameters roughly by 50%, which is sufficient to achieve almost perfect fit of the reference curve.

Parameter	Stopping precision on F	Average error [%]	Maximal error [%]
E	10^{-5}	0.41	1.23
ν	10^{-5}	0.16	2.20
$\bar{\sigma}_f$	10^{-2}	0.87	2.58
$\bar{K}$	10^{-2}	0.78	2.49
$\bar{\sigma}_f$	10^{-3}	0.30	0.59
$\bar{K}$	10^{-3}	0.49	1.54
$\bar{\bar{\sigma}}_f$	10^{-2}	0.47	1.32
$\bar{\bar{\beta}}$	10^{-2}	2.34	12.21
$\bar{\bar{\sigma}}_f$	3×10^{-3}	0.33	0.67
$\bar{\bar{\beta}}$	3×10^{-3}	0.26	2.68

Table 6: Influence of stopping precision on accuracy of identified parameters.

Finally, a similar conclusion holds for the parameters $\bar{\bar{\sigma}}_f$ and $\bar{\bar{\beta}}$ describing the softening part of the experiment. The stopping precision equal to 10^{-2} is too coarse to achieve sufficient precision on parameters and needs to be reduced to 3×10^{-3}. The effect of increased accuracy is then well visible in Figure 4b. This step completes the verification of the algorithm.
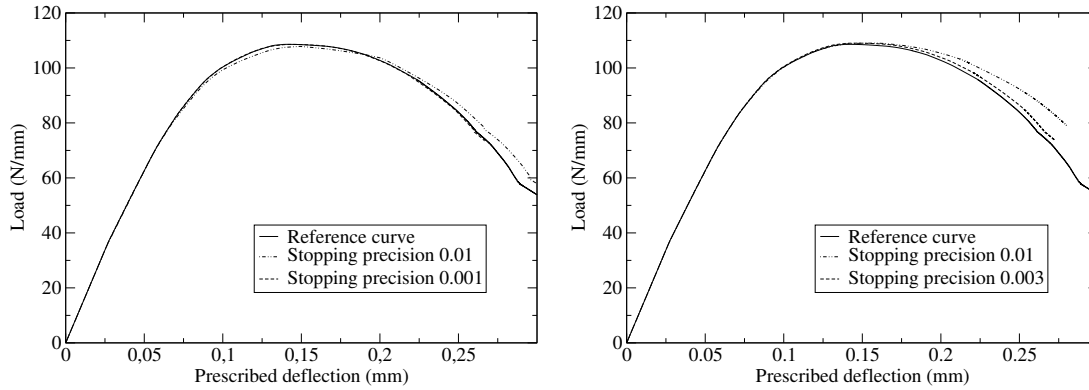

Figure 4: Comparison of load-deflection diagrams: (a) Hardening parameters (b) Softening parameters.

6 Conclusion

We have proposed a sound identification procedure for material parameters of the constitutive model for representing the localized failure of massive structures. The most pertinent conclusions can be stated as follows:

i) The sequential identification approach employed for the uniaxial tensile test (14) can be extended to the three-point bending test. The resulting algorithm is very straightforward and has a clear link with the structure of the constitutive model. Moreover, each of three stages uses only a part of the test simulation, which leads to substantial computational time savings.

ii) Due to the physical insight into the model, it was possible to construct simple objective functions F_1, F_2 and F_3 with a high sensitivity to the relevant parameters. This led to non-smooth and non-convex objective functions, which were optimized by robust soft-computing methods.

iii) The proposed identification procedure was verified on 100 independent optimization processes executed for each objective function. In the worst case, the reliability of the algorithm is 76% due to very small number of objective functions calls set in the termination condition. From our experience with evolutionary algorithms (6), such a result is rather satisfactory.

iv) As the result of a sequential character of the identification procedure, the errors in identified parameters accumulate. Therefore, the values need to be determined with higher accuracy then usually required in applications (i.e. 5%) and achievable by neural network-based inverse analysis (15).

v) The major difficulty of the proposed methods is to properly identify the three stages of structural behavior. From the point of view of method verification, where the reference load-deflection diagram is not noisy, the problem was successfully resolved. To fully accept the procedure, however, the experimental validation of the method appears to be necessary.

7 Acknowledgments

8 References

[1] D. Brancherie, P. Villon and A. Ibrahimbegovic. On a consistent field transfer in non linear inelastic analysis and ultimate load computation. *Computational Mechanics*, accepted for publication (2007).

[2] B. Chen and J. Liu. Experimental study on AE characteristics of three-point-bending concrete beams. *Cement and Concrete Research* **34** (2004), 391–397.

[3] D. Claire and F. Hild and S. Roux. A finite element formulation to identify damage fields: the equilibrium gap method. *Int. J. Numer. Meth. Engng (2004* 61:189–208.

[4] R. Furukawa and G. Yagawa. Inelastic Constitutive Parameter Identification Using an Evolutionary Algorithm with Continuous Individuals. *International Journal for Numerical Methods in Engineering* **40** (1997) 1071–1090.

[5] D. Goldberg. Genetic Algorithms in Search. *Optimization and Machine Learning*, Addison-Wesley, 1989.

[6] O. Hrstka, A. Kučerová, M. Lepš, and J. Zeman. A competitive comparison of different types of evolutionary algorithms. *Computers & Structures*, 81(18–19):1979–1990, August 2003.

[7] O. Hrstka and A. Kučerová, *Improvements of real coded genetic algorithms based on differential operators preventing the premature convergence*, Advances in Engineering Software **35** (2004), no. 3–4, 237–246.

[8] J. H. Holland, *Adaptation in Natural and Artificial Systems*, MIT Press, 1975.

[9] C. Iacono, L.J. Sluys, and J.G.M. van Mier. Estimation of model parameters in nonlocal damage theories by inverse analysis techniques. *Computer Methods in Applied Mechanics and Engineering*, 195(52):7211–7222, 2006.

[10] A. Ibrahimbegovic, C. Knopf-Lenoir, A. Kučerová, and P. Villon, *Optimal design and optimal control of elastic structures undergoing finite rotations*, International Journal for Numerical Methods in Engineering **61** (2004), no. 14, 2428–2460.

[11] A. Ibrahimbegovic. Mécanique non linéaire des solides déformables : Formulation théorique et résolution numérique par éléments finis. Lavoisier, Paris, 2006.

[12] M.K Karakasis and K.C Giannakoglou. On the use of surrogate evaulation models in multi-objective evolutionary algorithms. *ECCOMAS*, 2004.

[13] A. Kučerová and M. Lepš and J. Skoček, *Large black-box functions optimization using radial basis function networks*, In B. H. V. Topping, editor, Proceedings of Eighth International conference on the Application of Artificial Intelligence to Civil, Structural and Environmental Engineering, pages on CD-ROM, Stirling, United Kingdom, 2005. Civil-Comp Press.

[14] A. Kučerová and D. Brancherie and A. Ibrahimbegović. Material Parameter Identification for Damage Models with Cracks. *Proceedings of the Eighth International Conference on Computational Structures Technology* [CD-ROM]. Stirling: Civil-Comp Press Ltd, 2006.

[15] A. Kučerová and M. Lepš and J. Zeman. Back Analysis of Microplane Model Parameters Using Soft Computing Methods. *Computer Assisted Mechanics and Engineering Sciences*, 14(2), 2007, Accepted for publication.

[16] M. Lepš. Single and Multi-Objective Optimization in Civil Engineering. *Evolutionary Algorithms and Intelligent Tools in Engineering Optimization*, Southampton: WIT Press, 2005, 320–341.

[17] Z. Michalewicz, *Genetic Algorithms + Data Structures = Evolution Programs*, 3rd ed., Springer-Verlag, 1999.

[18] H. Nakayama and K. Inoue and Y. Yoshimon. Approximate optimization using computational intelligence and its application to reinforcement of cable-stayed bridges. *ECCOMAS*, 2004.

[19] D. Novák and D. Lehký. ANN inverse analysis based on stochastic small-sample training set simulation. *Engineering Applications of Artificial Intelligence*, 19(7):731–740, 2006.

[20] Z. Waszczyszyn and L. Ziemiański. Neurocomputing in the analysis of selected inverse problems of mechanics of structures and materials. *Computer Assisted Mechanics and Engineering Sciences*, 13(1):125–159, 2006.

[21] G. Yagawa and H. Okuda. Neutral networks in computational mechanics. *Archives of Computational Methods in Engineering*, 3(4):435–512, 1996.